The Royal Society

Protein crystal movements and fluid flows during microgravity growth

By Titus J. Boggon[1], Naomi E. Chayen[2], Edward H. Snell[3], Jun Dong[1,10], Peter Lautenschlager[4], Lothar Potthast[4], D. Peter Siddons[5], Vivian Stojanoff[6], Elspeth Gordon[7], Andrew W. Thompson[6,8], Peter F. Zagalsky[9], Ru-Chang Bi[10] and John R. Helliwell[1]

[1]*Structural Chemistry Section, Chemistry Department, University of Manchester, Oxford Road, Manchester M13 9PL, UK*
[2]*Department of Biophysics, The Blackett Laboratory, Imperial College of Science, Technology and Medicine, London SW7 2BZ, UK*
[3]*NASA, Laboratory for Structural Biology, Code ES76, Building 4464, MSFC, Huntsville, AL 35812, USA*
[4]*Dornier GmbH, Raumfahrt-Infrastruktur, 88039 Friedrichshafen, Germany*
[5]*NSLS, Brookhaven National Laboratory, Upton, NY 11973, USA*
[6]*ESRF, BP 220, 38043 Grenoble Cedex, France*
[7]*Laboratoire de Cristallographie Macromoleculaire, Institut de Biologie Structurale, 41 Avenue des Martyrs, 38027 Grenoble Cedex, France*
[8]*EMBL, Ave. des Martyrs, 38043 Grenoble Cedex, France*
[9]*Biochemistry Department, Royal Holloway and Bedford New College, University of London, Egham, Surrey TW20 0EX, UK*
[10]*Institute of Biophysics, Academia Sinica, Beijing 100101, China*

The growth of protein crystals suitable for X-ray crystal structure analysis is an important topic. The methods of protein crystal growth are under increasing study whereby different methods are being compared via diagnostic monitoring including charge coupled device (CCD) video and interferometry. The quality (perfection) of protein crystals is now being evaluated by mosaicity analysis (rocking curves) and X-ray topographic images as well as the diffraction resolution limit and overall data quality. Choice of a liquid–liquid linear crystal-growth geometry and microgravity can yield a spatial stability of growing crystals and fluid, as seen in protein crystallization experiments on the uncrewed platform EURECA. A similar geometry used within the Advanced Protein Crystallization Facility (APCF) onboard the crewed shuttle missions SpaceHab-01 and IML-2, however, has shown by CCD video some lysozyme crystal movement through the mother liquor. Moreover, spurts and lulls of growth of a stationary lysozyme protein crystal that was probably fixed to the crystal-growth reactor wall suggests *g*-jitter stimulated movement of fluid on IML-2, thus transporting new protein to the growing crystal faces. In yet another study, use of a hanging drop vapour diffusion geometry on the IML-2 shuttle mission showed, again via CCD video monitoring, growing apocrustacyanin C_1 protein crystals executing near cyclic movement, reminiscent of Marangoni convection flow of fluid, the crystals serving as 'markers' of the fluid flow. These observations demonstrated that the use of vapour diffusion geometry did not yield spatially stable crystal position or fluid conditions for a solely protein diffusive regime to be realized. Indeed mosaicity evaluation of those vapour diffusion-grown apocrustacyanin C_1 crystals showed

Phil. Trans. R. Soc. Lond. A (1998) **356**, 1045–1061
Printed in Great Britain

inconsistent protein crystal quality, although the best crystal studied was microgravity grown. In general, realizing perfect conditions for protein crystal growth, of absence of movement of crystal or fluid, requires not only the correct choice of geometry but also the avoidance of low-frequency ($\lesssim 5$ Hz) g-jitters. A review is given here of existing results and experience over several microgravity missions. Some comment is given on gel protein crystal growth in attempts to 'mimic' the benefits of microgravity on Earth. Finally, the recent new results from our experiments on the shuttle mission LMS are described. These results include CCD video as well as interferometry during the mission, followed, on return to Earth, by reciprocal space mapping at the NSLS, Brookhaven, and full X-ray data collection on LMS and Earth control lysozyme crystals. Diffraction data recorded from LMS and ground control apocrustacyanin C_1 crystals are also described.

Keywords: protein crystallization; microgravity; interferometry; CCD video; crystal perfection; g-jitter; Marangoni convection

1. Background

The monitoring of crystal growth using CCD video allows key data to be collected on the process of crystallization, such as growth rates and movements of crystals (figure 1). Clearly then, crystallization geometries can be directly compared as well as the 'quality' of individual missions, along with Earth control conditions. Moreover, the state of the mother liquor can be monitored via interferometry, which measures refractive index changes which can be due to the flows of, for example, precipitating agents like salt, and subsequently gradual depletion of protein as crystals nucleate and grow.

Harvesting of crystals is made on return to Earth from a microgravity mission where a variety of X-ray analyses can be conducted, especially using high brilliance synchrotron X-ray sources in order to combine fine collimation and strong intensity to probe weak reflections. Hence, mosaicity measurements, as well as X-ray topographic images, can be collected, crystal quality compared and further insights gained into the various crystallization methods and their relative success.

2. Resumé of previous experiments onboard shuttle missions

Apocrustacyanin C_1 crystal growth in vapour diffusion geometry was conducted on the IML-2 (STS-65), USML-2 (STS-73) and LMS (STS-78) shuttle missions. The experiments were monitored with CCD video observation (Chayen *et al.* 1997) and thereby provided some insights into the effects of Marangoni convection on the crystallization process in microgravity.

Lysozyme crystal growth has been conducted using the dialysis membrane technique (in dialysis geometry crystallizations there is no gas–liquid phase boundary) provided by the APCF onboard the SpaceHab-01 (STS-57) and IML-2 (STS-65) as well as recently on the LMS (STS-78) shuttle missions. The APCF (Advanced Protein Crystallisation Facility) is a multiuser facility built by Daimler–Benz Aerospace–Dornier under the contract of the European Space Agency ESA. Significant crystal movements were viewed on all these missions. However, in relation to the Marangoni convections described below these movements are generally slight, with one exception. On SpaceHab-01, well into the mission, and after crystal growth had largely

been completed, a sudden and dramatic motion of the crystals occurred attributed to the retrieval of the EURECA satellite (see below).

The CCD video in the APCF can view crystallizations using either a wide field-of-view (WFOV) or a narrow field-of-view (NFOV) lens (Bosch *et al.* 1992; Snyder *et al.* 1991). The lenses are non-interchangeable, and therefore a specified crystallization can be monitored only using either WFOV or NFOV optics. WFOV monitors the whole protein chamber ($6.48 \times 8.59\ \mathrm{mm}^2$), whereas NFOV monitors only a magnified portion ($3.77 \times 4.99\ \mathrm{mm}^2$). Due to the constraints (power limitation) placed upon the apparatus, recording of the digital images takes a period of about 4 min. This, combined with moving the camera to view other reactors, has restricted the frequency of images that can be obtained.

(*a*) *Apocrustacyanin C_1 on the IML-2 and USML-2 missions*

Apocrustacyanin C_1 has been crystallized on the IML-2, USML-2 and LMS shuttle missions. On IML-2, CCD video was used to follow the crystallization. Crystals grew in the vapour diffusion droplet and moved in a circular way, consistent with that of Marangoni convection (Chayen *et al.* 1997; Savino & Monti 1996) (figure 1*a*). The images also display a 'halo' effect around the growing crystals which is attributed to the presence of depletion zones (i.e. solution regions which are depleted of this coloured protein). The crystals from the USML-2 mission (which were not monitored by CCD video) underwent an X-ray mosaicity analysis. The quality enhancement between Earth-grown and microgravity-grown crystals was not as marked as for the lysozyme crystals grown in dialysis geometry, nor was it consistent between the two populations, although the best crystal was microgravity grown (Snell *et al.* 1997*a*).

(*b*) *Lysozyme on the SpaceHab-01 mission*

WFOV CCD video monitored lysozyme crystallization in one experimental reactor onboard SpaceHab-01. Although the images do not have a particularly high sampling frequency (about 8 h between each image), and a very detailed examination has not taken place, it was notable that a bulk sedimentation of crystals occurred at the time the EURECA satellite was retrieved. The gravitational acceleration at that moment onboard the shuttle was in excess of 1300 μg, i.e. mg. X-ray mosaicity analyses of the crystals grown on this mission showed the most perfect protein lipids ever seen (minimum mosaicity observed was 0.001°). An approximate three times improvement in crystal perfection over the ground controls was seen (Snell *et al.* 1995; Helliwell *et al.* 1996) consistent also with the lysozyme grown on the IML-2 mission (described in the next section). Riès-Kautt *et al.* (1997) state that lysozyme crystals grown on the ground and in microgravity show no significant differences in rocking curve; their minimum observed mosaicity was 0.006°.

(*c*) *Lysozyme on the IML-2 mission*

In the IML-2 mission one crystallization experiment was monitored using NFOV optics. A series of nine images at different focal lengths were taken over a 40 min period, followed by an 8 h wait until the next series of images was taken. We were able to conduct two CCD video analyses from these data (Snell *et al.* 1997*b*). First, a crystal nucleated, probably attached to the chamber wall, within the field of view. Analysis of this crystal revealed spurts and lulls in its growth rate (figure 2). The times of the spurts in crystal growth rate directly correlated with those of astronaut exercise periods. Analysis of gravitational accelerations onboard the orbiter showed

(*a*)

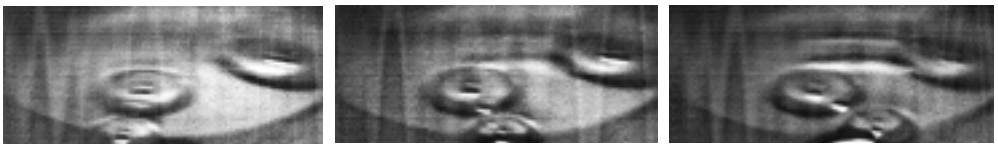

(*b*)

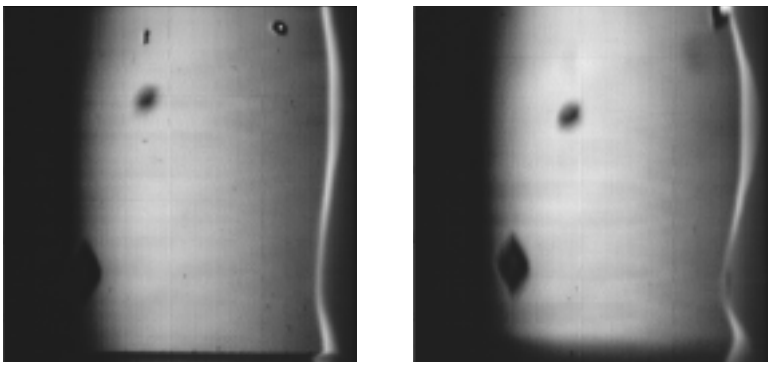

Figure 1. Examples are given from different microgravity missions in which we have been involved. (*a*) Cyclic movements of apocrustacyanin C_1 crystals monitored by CCD video on the IML-2 shuttle mission, using a vapour diffusion geometry in the APCF, shown here over a period of 9 min. (*b*) Near linear drift movements of lysozyme crystals monitored by CCD video on the IML-2 shuttle mission, using a liquid–liquid dialysis geometry onboard the APCF. Time between these two frames is 36 min.

that astronaut exercise periods, especially the use of an ergometer (a bicycle-type device), produced periods of *g*-jitter approaching 1000 μg. It seems that the increased gravity of these periods induced movements of fluids within the crystallization chamber, thus transporting new protein to the growing crystal faces. In our second video analysis three crystals free floating in solution were tracked over 40 min periods, between the first and last focal length images (figure 1*b*). The speeds of the crystal movements were seen to be of the order of 200 $\mu m\,h^{-1}$, and in the same direction for all three crystals, covering a total distance of *ca.* 0.3 mm in *ca.* 40 min (i.e. the order of one crystal width). Table 1 compares such experimentally measured speeds of crystals and distances travelled. X-ray mosaicity analysis of the crystals grown on this mission showed a three times improvement in crystal perfection over the ground controls, although none of the crystals were as perfect as those from the shorter SpaceHab-01 mission, but which were also three times more perfect than their Earth-grown controls (Snell *et al.* 1995; Helliwell *et al.* 1996).

3. The EURECA uncrewed satellite and α-crustacyanin protein crystal growth

We have also analysed protein crystal growth onboard an uncrewed platform, whereby α-crustacyanin was grown on the ESA's EURECA satellite using a liquid–liquid free interface diffusion geometry. The apparatus and experiment is described elsewhere (Zagalsky *et al.* 1995; Snyder *et al.* 1991; Schmidt *et al.* 1992). We noted that for long periods of time (7 weeks) the free floating crystals nucleated and then

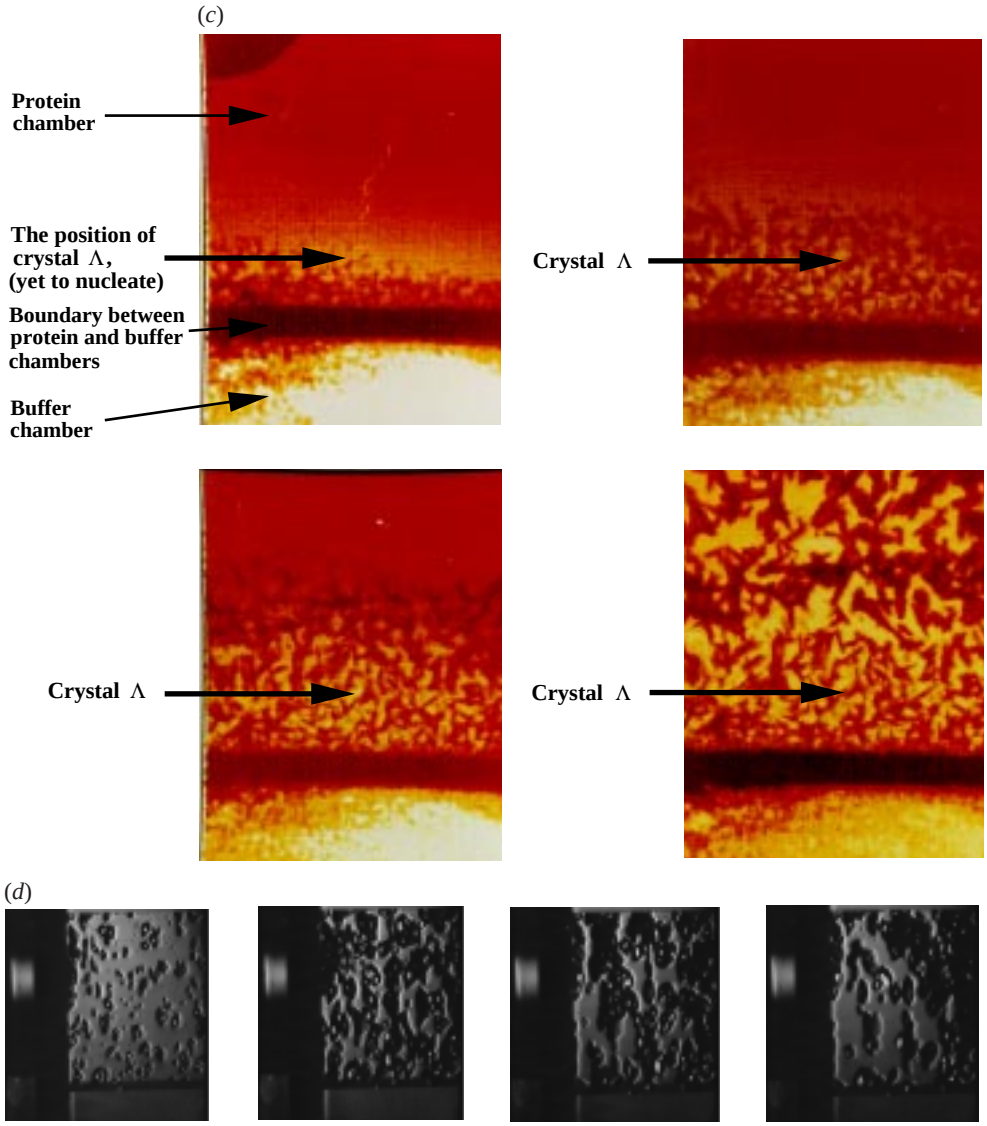

Figure 1. *Cont.* (*c*) Video images of α-crustacyanin crystal growth, in free interface liquid–liquid geometry, onboard the uncrewed satellite EURECA. The top two frames and the one at bottom left span 38 h and the one at bottom right was 26 days later. *Λ* indicates an easily recognized crystal that is seen to remain stationary throughout the period shown. *Stationary* crystal growth is seen over a period of 7 weeks in fact. (*d*) Near linear drift movements of lysozyme crystals monitored by CCD video on the LMS shuttle mission, using a liquid–liquid dialysis geometry onboard the APCF (see also figure 5). The crystal drift is towards the top of the reactor and from left to right. These four frames span the 15 days of the mission.

grew without moving (Boggon *et al.* 1998) (figure 1*c*), and were only finally disturbed by failures of the temperature control system. Analysis of the gravitational acceleration environment showed that a maximum of only 62.5 μg (Eilers & Stark 1993) was experienced onboard the uncrewed platform. This maximum gravitational acceleration was an order of magnitude lower than that experienced by crystal-growth

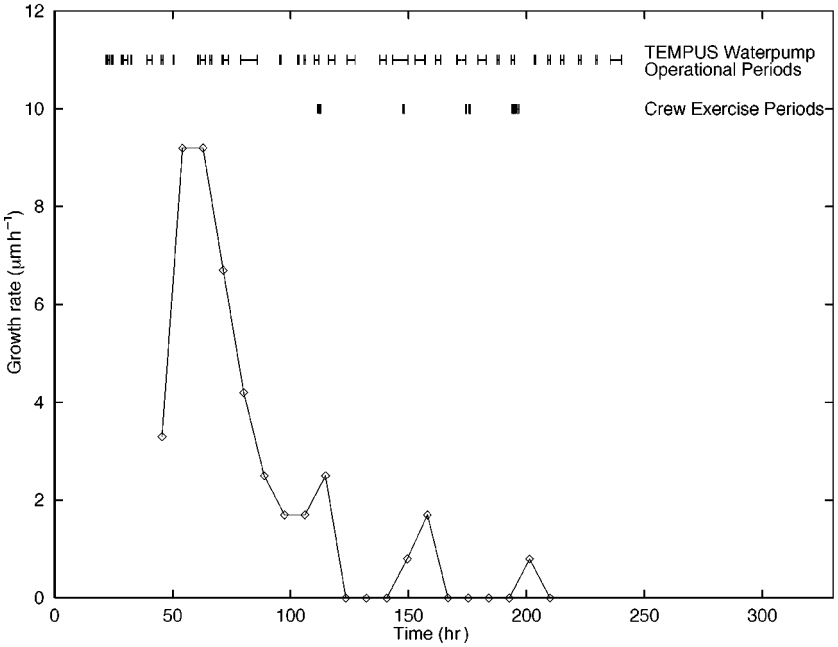

Figure 2. Spurts and lulls in growth show a correlation with astronaut exercise periods (*ca.* 5 Hz, plus harmonics, *g*-jitter) presumably inducing fluid flow and revived transport of protein to the growing protein crystal. These are possible explanations of the mosaic blocks seen in topographic images (see Chayen *et al.* (1996) and figure 7).

experiments onboard the crewed Space Shuttle described above. The spatial stability of the crystals grown onboard EURECA corresponds then to a spatial coherence length of at least as small as 1–2 CCD pixels (*ca.* 25–50 μm) (and probably better than this) for the fluid over 7 weeks. This is clearly the degree of crystallization stability, of the crystals and fluid, that can be aimed for. Indeed, the crystals grown on this mission were bigger, and had a better morphology than seen on Earth before (Zagalsky *et al.* 1995). It was most unfortunate that the experimental temperature regulation apparatus failed and temperatures as high as 40 °C were experienced by the crystals.

4. Crystal growth in gels

Crystallization in gels can suppress fluid and crystal movement following nucleation. Moreover, the rate of growth can be reduced and might then generally lead to larger, higher-quality crystals of enhanced stability. Presumably these effects could arise from the decreased mobility of the macromolecules and their flux at the crystal surface during growth, similar to microgravity.

In particular, by reducing or eliminating density-driven and Marangoni convective flow patterns, a more controlled environment may be generated around crystal-growth surfaces. The sedimentation of nucleated crystals is minimized within the gel matrix. Interestingly (figure 3) the number of crystal nucleation sites may be reduced in gels, depending on the gel material (Provost & Robert 1991). Our gel-grown crystals are grown as follows. The gel used was a physical hydrogel of agarose at a concentration 0.2%. The hen egg-white lysozyme concentration was 25 mg ml^{-1} in the buffer, which consisted of sodium acetate and acetic acid (pH 4.5); the salt

Table 1. *Experimental speeds and distances travelled of microgravity-grown protein crystals for the cases shown in figure 1*

(FID, liquid–liquid free interface diffusion; DIA, liquid–liquid dialysis; VAD, vapour diffusion (hanging drop).)

mission	protein	crystallization geometry	time period	speed (μm s^{-1})	total observed movement
IML-2	apocrustacyanin C_1	VAD	8 min 45 s	2.1[§]	1.08 mm
IML-2	lysozyme	DIA	*ca.* 40 min periods	0.05	0.3 mm
EURECA	α-crustacyanin	FID	7 weeks	*ca.* 0[†]	*ca.* 0[†]
LMS	lysozyme	DIA	24–260 h[‡]	0.004[*]	0.42–3.38 mm[‡]
			ca. 2 h[a]	0.026[⋆]	0.21 mm
			ca. 2 h[b]	0.027[⋆]	0.17 mm
			ca. 2 h[c]	0.031[⋆]	0.19 mm

[§]This observation compares well with theoretical estimates (table 2).

[†]The movement of crystals, for a 7 week period was less than 1–2 pixels (i.e. less than 25–50 μm); thereafter problems with the cooling elements caused crystal movements.

[*]0.004 μm s^{-1} = 40 Å s^{-1}.

[‡]For each crystal analysed as shown in figure 5.

[⋆]Instantaneous speed for all crystals over the time periods: (a), MET 3/02:35–3/04:47; (b), MET 4/04:48–4/06:31; (c), MET 6/01:18–6/03:01.

Table 2. *Theoretical estimates for lysozyme crystal speeds for vapour diffusion (Savino & Monti 1996)*

location	geometry	speed (μm s^{-1})
Earth	hanging droplet ('half')	5
Earth	sitting droplet ('half')	15
0g	'full' droplet	500

solution consisted of sodium chloride. A small amount of MPD was added to the protein solution. The glass tube used was 6 cm tall with an inner diameter of 4 mm. These crystals await detailed mosaicity, topography and resolution limit testing at the time of writing. Other gel crystal-growth experiments have been performed on acidic phospholipase A_2 in attempts to mimic the environment of microgravity (Bi 1997).

5. Recent LMS mission results

Four lysozyme crystallizations were carried out in microgravity on the LMS mission, and four identical experiments were conducted as ground controls during the period of the LMS mission. The ground control crystallizations were set up at the same time, and using the same solutions, as those of the mission. All parameters

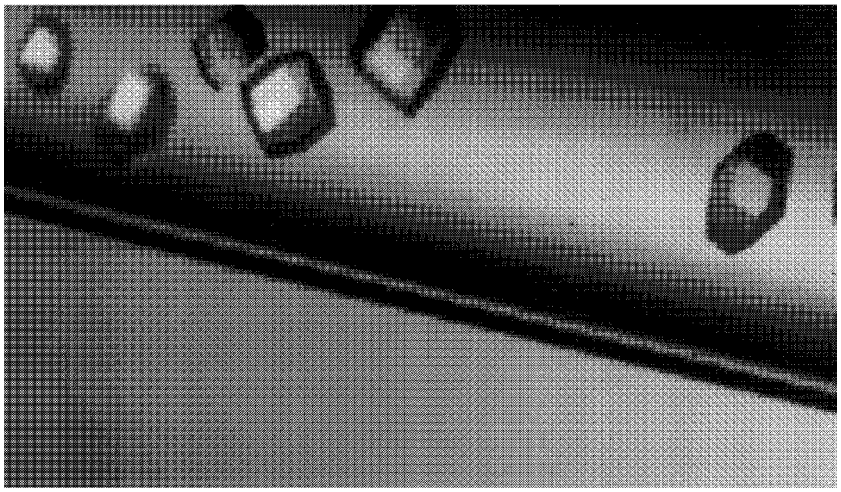

Figure 3. Gel-grown hen egg-white lysozyme crystals.

were kept as identical as possible to the microgravity case, although a temperature stability during growth of $20 \pm 0.1\,^{\circ}\mathrm{C}$ was not possible, and $\pm 1\,^{\circ}\mathrm{C}$ was used. Two crystallization conditions, one with a higher precipitant concentration, and one with a 7% lower precipitant concentration were used. Two microgravity reactors were monitored using Mach–Zehnder interferometry and CCD video, the other two microgravity reactors could not be visually monitored during the mission. All reactors produced crystals. A variety of X-ray evaluations were conducted on these crystals.

(*a*) *CCD video*

On the LMS mission two reactors were monitored using CCD video, they were numbered reactors 7 and 9 in the APCF. For reactor 7, WFOV images of the whole protein chamber were taken at one focal length position every 2 h, beginning 15 h after activation of the APCF. In reactor 9, the first image was taken 90 h after APCF activation. CCD video analysis of these two reactors complemented Mach–Zehnder interferometry analysis (§ 5 *b*).

The monitoring of reactor 7 showed that nucleation events occurred depending on the spatial position within the reactor, with the first crystals visible 25 h 37 min after APCF activation close to the dialysis membrane (figure 4). We noted significant crystal 'drifting' movements (figure 5) throughout the mission, whereby nucleation events occurred throughout the chamber but were very quickly followed by a global sedimentation drift towards the top of the reactor. The only crystals that remained in their nucleation positions were those that grew on the chamber walls. By following 20 different crystals for the periods that they could be accurately tracked sudden global movements could also be seen, in addition to the steady drift, at the 76, 102 and 145 h points, as well as other times. The source of the sudden disturbance at these times into the LMS mission is being investigated. The total drift distance, for all 20 crystals analysed, over the periods they were analysed, ranged between 0.42 and 3.38 mm, with an average speed of *ca.* $0.004\ \mu\mathrm{m\ s^{-1}}$ ($40\ \mathrm{\AA\ s^{-1}}$).

(*b*) *Mach–Zehnder interferometry*

On the LMS mission, the two reactors described above were also monitored using Mach–Zehnder interferometry. Reactor 7 contained a slightly higher precipitant con-

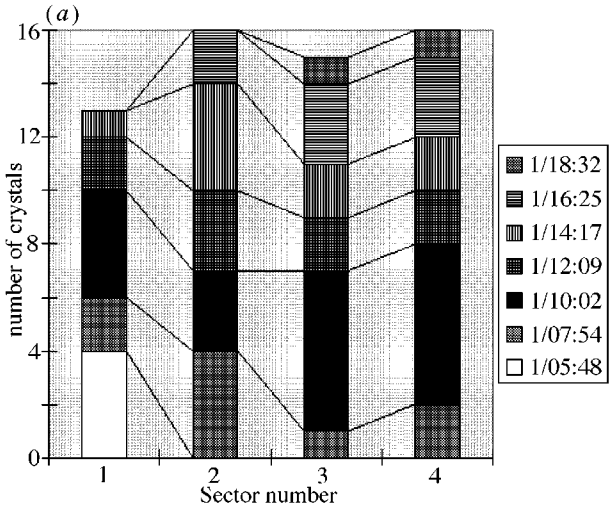

Figure 4. (*a*) The dependence of spatial position of nucleation of crystals. The different shades of the bars correspond to the number of crystals that have nucleated by that time (see the key in days/hours: minutes) within each of the four sectors.

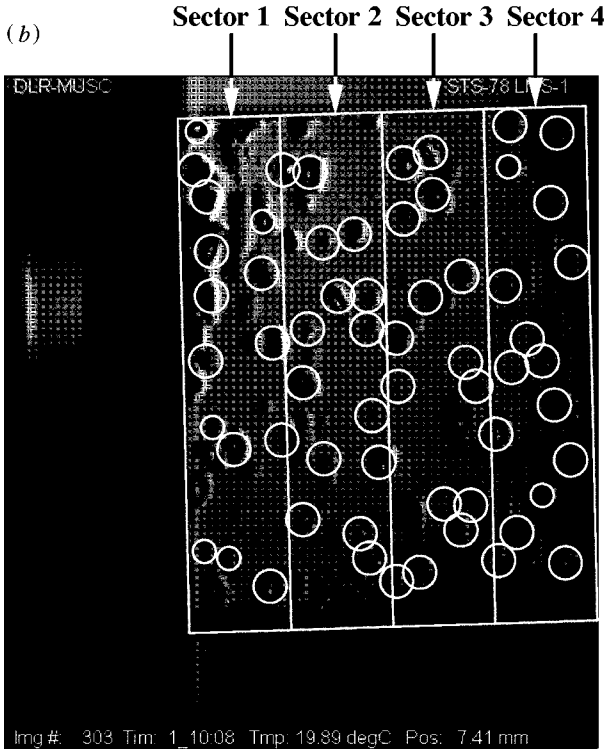

Figure 4. *Cont.* (*b*) Shows the four sectors referred to in (*a*) within the reactor with the crystals monitored circled.

centration and so it was monitored at a slightly faster rate to compensate for the expected increased speed of equilibration of precipitant. Due to time constraints on digitally recording the images (as with the CCD video, 4 min per whole image), and

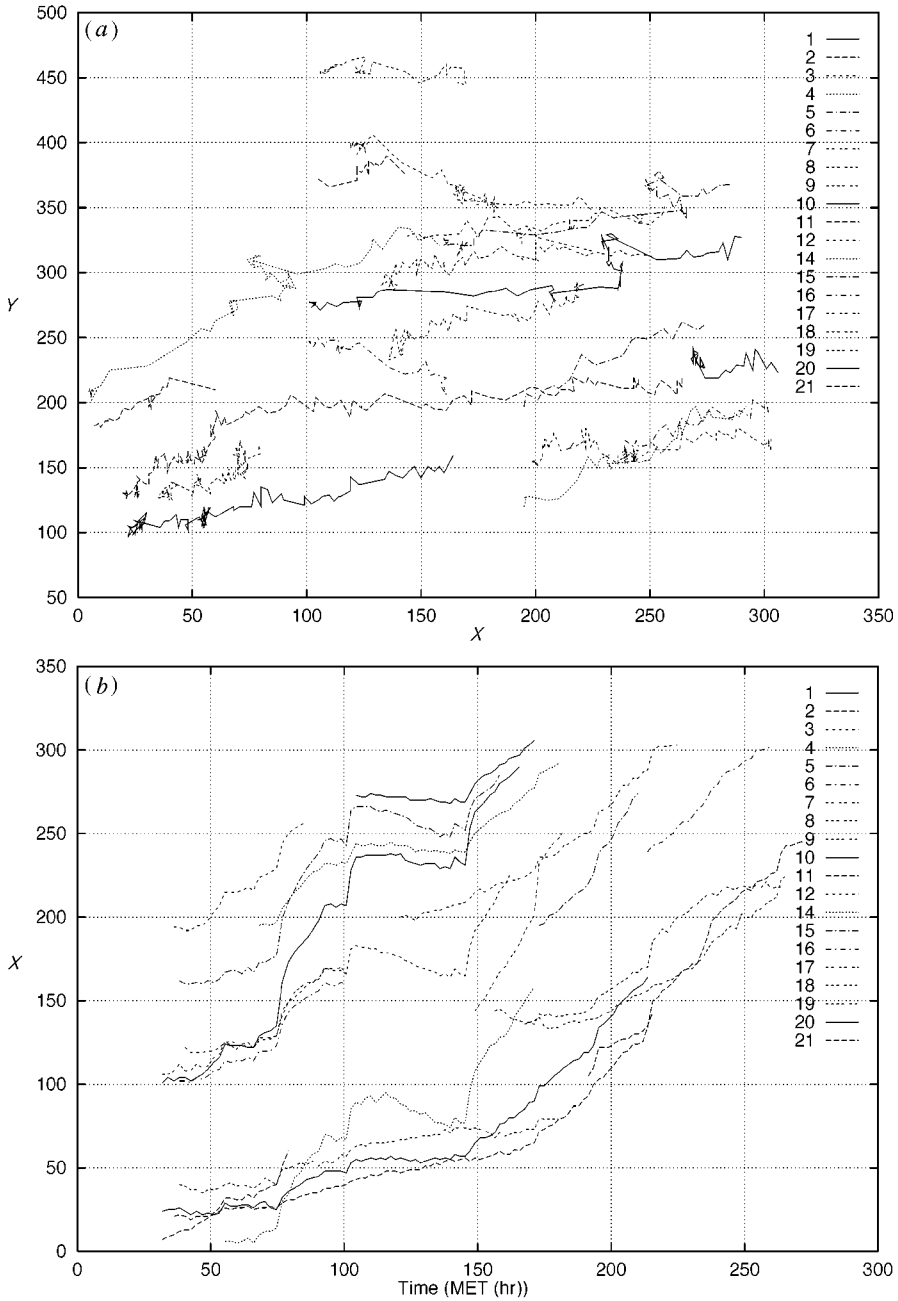

Figure 5. Crystal movement throughout the LMS mission in reactor 7. Three graphs illustrating the movements of 20 crystals are shown. Graph (*a*) shows X versus Y, (*b*) X versus time. The units are pixels and hours (mission elapsed time, MET). The positions of crystals in figure 5*a* can be overlayed onto figure 1*d*.

the need to accurately follow the progression and number of fringes, whole interferograms could not be collected for the first 15 h after APCF activation. Instead two windows were defined (w1 and w2 in figure 6*a*), which monitored the local average

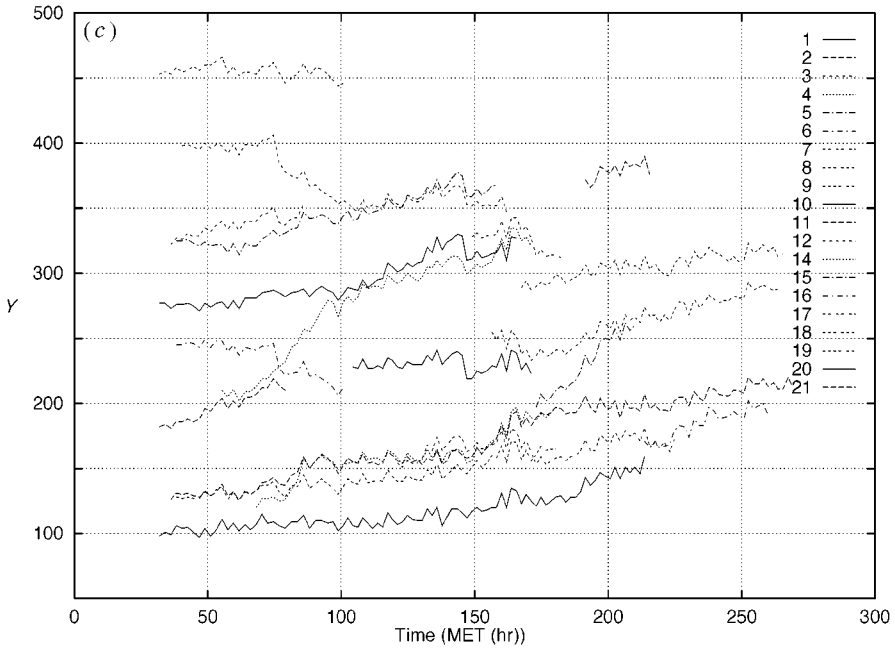

Figure 5. *Cont.* (*c*) Y versus time.

grey value at 4 or 6 min intervals for reactors 7 and 9, respectively. After 15 h, whole reactor interferograms were collected at 11 min intervals for both reactors.

Unfortunately the laser was unsteady, and mode switching occurred throughout the mission. This was problematic, especially in the first 15 h, when average grey values were the only method of analysis. Consequently, some fringes were probably missed in that period. However, a more complete analysis was possible with the whole interferograms collected after the 15 h point, although these also have been affected by the problematic laser (figure 6).

There was, however, enough data to yield some very interesting results. First, the direction of fringe movement reversed at about the 8 h point in both reactors, and then again at the point that crystals became visible in the CCD video monitoring, i.e. between 25 and 31 h (depending on the position within the protein chamber) (figure 6*e*). Compared to the solitary reversal in fringe movement direction present in the ground control experiments (Snell *et al.* 1996), this is a surprising result which suggests a different pre- and post-nucleation process occurs in microgravity compared to the Earth-grown case. This must be looked at further.

Finally, the whole chamber interferograms demonstrated the stability of fluid within microgravity crystallization by showing an effect that is rarely seen using Mach–Zehnder interferometry on Earth, namely depletion zones are clearly visible around growing crystals (figure 6*b*, *d*).

(*c*) *Crystal perfection assessment using X-ray reciprocal space mapping and topographic techniques*

Synchrotron X-ray analysis was carried out at the NSLS using beamline X26C on the LMS crystals. Protein crystal mosaic spread measurements by use of rocking curves is an indicator of the internal physical perfection present (Helliwell 1988). The addition of an analyser crystal between the sample and detector enables recip-

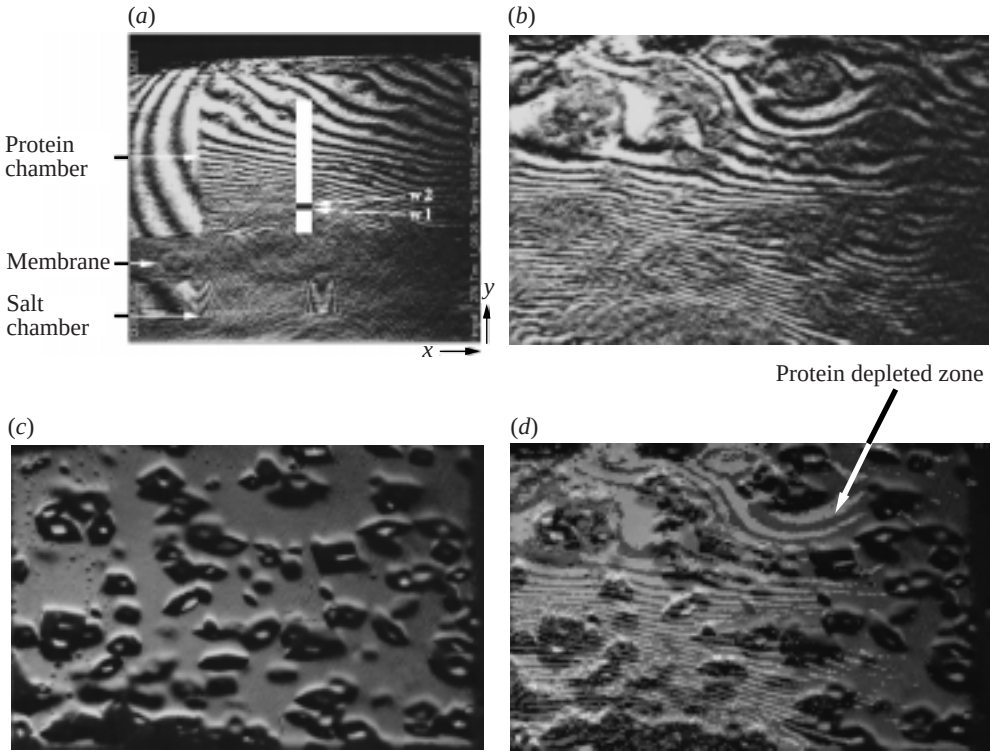

Figure 6. Diffusion of precipitating agent into the protein chamber of a crystallization reactor and subsequent 'removal' of protein into nucleating and then growing crystals can be monitored via Mach–Zehnder interferometry. (*a*) An example of a whole interferogram with interference fringes clearly visible. The two grey value measuring windows are marked as w1 and w2, and the white strip indicates the area analysed in (*e*). (*b*) A fringe image, later into the crystallization. (*c*) A CCD video image taken at the same time as the fringe image (*b*). (*d*) Overlay of (*b*) and (*c*) showing a protein depletion zone (marked).

rocal space mapping of ω, the sample axis, and ω', the analyser axis (Snell 1998). Reciprocal space maps along one axis provide a measure of pure mosaicity effects (volume and orientation), and along the other axis strain effects. Combination of the use of this technique with X-ray topography (Stojanoff *et al.* 1996, 1997), can produce a finely detailed picture of a single reflection, and an in-depth knowledge of the internal order of the crystal. Two examples are shown here (figure 7).

(*d*) *The X-ray data collection from the LMS and ground control lysozyme and apocrustacyanin C_1 crystals, under identical laboratory X-ray source conditions*

Complete X-ray single crystal diffraction data sets were measured on one LMS lysozyme and one Earth control crystal sample. Details of the data processing are given in table 3. Table 4 is a similar analysis for apocrustacyanin C_1, but where a large difference in crystal volume is the predominant effect. The procedures followed for data collection were essentially identical for the microgravity and Earth lysozyme cases. The data quality from the microgravity and Earth control lysozyme crystals is essentially identical using coarse angle rotation ranges. For the LMS microgravity-grown lysozyme crystal the data collection protocol was as follows: 60° of 0.75°

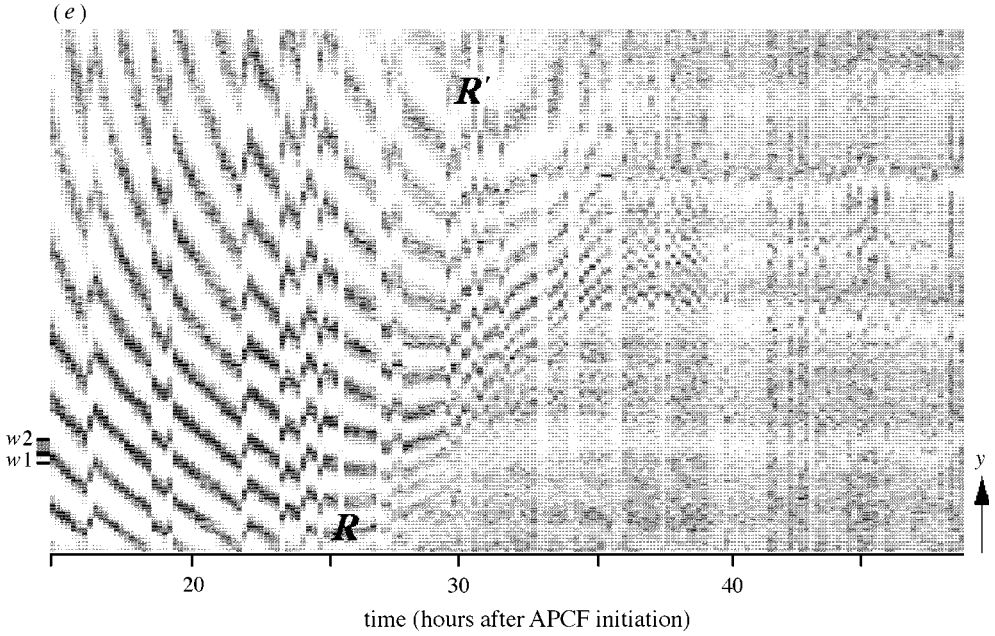

Figure 6. *Cont.* (*e*) Analysis of the movement of fringes within the white strip shown in figure 6*a*. The average grey value of pixels in x within the white strip has been obtained and shown here as a single pixel. The height (y) is unchanged for both sets of pixels.

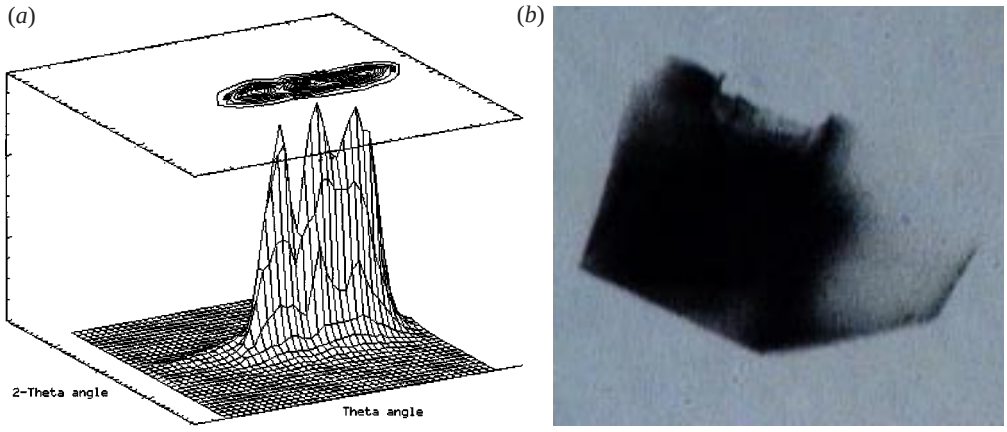

Figure 7. Protein crystal quality assessment via (*a*) reciprocal space mapping and (*b*) topographic images for lysozyme crystals grown aboard the LMS shuttle mission as examples.

oscillations at a distance of 250 mm using 30 min exposures, followed by 60° of 0.50° oscillations at a distance of 300 mm using 20 min exposures. For the Earth-grown crystal the data collection protocol was identical, and then in addition 60° of 1.5° oscillations at a distance of 450 mm using 30 min exposures were recorded. The LMS crystal was $0.50 \times 0.50 \times 0.35\ \mathrm{mm}^3$ ($0.0875\ \mathrm{mm}^3$) and the Earth control crystal was $0.70 \times 0.50 \times 0.45\ \mathrm{mm}^3$ ($0.1575\ \mathrm{mm}^3$).

Resolution limits are dependent on the data collection source and measuring conditions. In earlier work on lysozyme, use of the Swiss–Norwegian beamline at the

Table 3. *X-ray data sets collected on LMS and LMS ground control lysozyme crystals on the Manchester R-AXIS IIc IP area detector MoKα ($\lambda = 0.71$ Å wavelength)*

(Overall I/Sigma I for LMS is 15.7, for LMS ground control is 16.5. Crystal volume for LMS is 0.0875 mm^3, and for LMS ground control is 0.1575 mm^3.)

	LMS		LMS ground control	
resolution	R_{merge}	completeness %	R_{merge}	completeness %
99.00–4.19	0.054	95.1	0.056	98.8
4.19–3.33	0.064	98.8	0.064	99.2
3.33–2.91	0.075	99.2	0.070	97.1
2.91–2.64	0.085	99.6	0.080	97.5
2.64–2.45	0.093	99.9	0.090	96.6
2.45–2.31	0.093	99.6	0.090	97.7
2.31–2.19	0.099	99.3	0.097	96.9
2.19–2.10	0.105	98.1	0.105	96.1
2.10–2.02	0.120	94.3	0.116	94.9
2.02–1.95	0.135	88.8	0.139	92.1
1.95–1.89	0.165	77.3	0.163	88.7
1.89–1.83	0.186	66.5	0.187	81.4
1.83–1.78	0.239	62.1	0.249	70.9
1.78–1.74	0.271	54.5	0.255	64.3
1.74–1.70	0.393	45.1	0.344	56.1
overall	0.072	85.5	0.069	88.8

ESRF and an extra fine ω step diffractometer ($\delta\omega \approx 10^{-4}$ deg) yielded reflections at 1.2 Å for microgravity lysozyme but not the Earth-grown crystals (see figures 3 and 4 of Snell *et al.* (1995)). This can be contrasted with the resolution limit here for laboratory data sets of LMS lysozyme crystals of *ca.* 1.7 Å. The full exploitation of the crystal perfection available is very difficult if step widths of 10^{-4} degrees are required. Nevertheless, new area detectors like the pixel detector could exploit such quality (Chayen *et al.* 1996) when used in conjunction with X-ray undulator sources, which have extremely fine collimation in horizontal *and* vertical directions. (For a discussion of detector and synchrotron radiation sources for macromolecular crystallography see Helliwell (1992).) It is the geometric quality and internal perfection as well as the sizes of protein crystals, which multiplied together (i.e. mosaicity × sample size) form the parameter (sample acceptance) that is comparable directly with synchrotron machine emittance. Earlier work comparing mosaicity of microgravity and Earth-grown crystals of lysozyme and apocrustacyanin C_1 can be found in Helliwell *et al.* (1996) and Snell *et al.* (1995, 1997*a*). Examples of topographs of Earth- and microgravity-grown lysozyme can be found in Stojanoff *et al.* (1996) and Chayen *et al.* (1996).

6. Conclusions

Microgravity protein crystal growth can enable the crystallization process to proceed in a relatively undisturbed state, with diffusion dominating rather than fluid

Table 4. *Resolution limits of apocrustacyanin C_1 crystals grown onboard the LMS missions in a vapour diffusion reactor and Earth-grown controls determined from 1° oscillation images using ESRF BL19.*

	LMS		LMS ground control	
resolution	R_{merge}	completeness %	R_{merge}	completeness %
25.00–4.92	0.048	86.5	0.045	97.2
4.92–3.91	0.048	91.0	0.047	99.0
3.91–3.42	0.050	92.6	0.070	99.5
3.42–3.11	0.051	94.2	0.089	99.8
3.11–2.88	0.058	94.7	0.130	99.9
2.88–2.71	0.064	95.0	0.172	99.7
2.71–2.58	0.070	95.3	0.203	99.8
2.58–2.47	0.074	96.6	0.230	99.6
2.47–2.37	0.075	96.1	0.239	99.9
2.37–2.29	0.084	95.2	0.266	99.5
2.29–2.22	0.084	97.9	0.265	99.7
2.22–2.15	0.085	95.7	0.275	99.1
2.15–2.10	0.086	98.1	0.317	98.6
2.10–2.05	0.094	95.3	0.358	98.9
2.05–2.00	0.104	98.2	0.403	98.2
Overall	0.056	94.7	0.110	99.2

ESRF BL19 is a bending magnet source beamline. Operating parameters during data collection were $\lambda = 0.7513$ Å; CCD detector (image intensifier type), exposure times 30 s, rotation angles 1°, $\delta\lambda/\lambda \sim 10^{-4}$. Overall I/Sigma I for LMS is 30.4, and for ground control is 9.5. LMS crystal volume is 0.0432 mm^3, ground control crystal volume is 0.0034 mm^3.
Data collection of an Earth-grown crystal on ESRF BL4 gave diffraction to 1.3 Å. The crystal's dimensions were $0.2 \times 1.25 \times 0.5\ \mathrm{mm}^3$ ($0.125\ \mathrm{mm}^3$). ESRF BL4 is fed by an X-ray undulator source (horizontal and vertical divergences of the beam *ca.* 0.005°, i.e. 0.1 mrad). Detector used Mar IP, exposure times 30 s, rotation angles 1°, $\lambda = 0.94$ Å, $\delta\lambda/\lambda \sim 10^{-4}$.
The positive influence of a stronger beam, and a bigger crystal volume is illustrated by the effects on the resolution limits of these crystals, i.e. in the main table 4, as well as the BL4 test.

flow. The closest to this ideal situation has come from the use of a linear liquid–liquid free interface diffusion crystallization geometry and on an uncrewed platform in microgravity (EURECA). Use of vapour diffusion hanging drops is prone to crystal movements which have the form of Marangoni stimulated fluid flows. It would be a pity if hanging drops could not be used in microgravity, due to Marangoni fluid flow, since it is a method rather economical of protein. Fortunately, there are other micromethods that might be tried in microgravity, which avoid the liquid–vapour interface, and thereby Marangoni convection. In addition, *g*-jitter events (especially at low frequencies) appear to stimulate crystal movements and also fluid flows. The overall drift speed of lysozyme crystals on the LMS shuttle mission of 40 Å s^{-1} presumably is tolerable but is of interest in modelling the biophysical chemistry of protein crystal growth. However, the cases of sudden jumps on LMS of, for example, *ca.* 0.2 mm over 2 h periods (i.e. 0.03 µm s^{-1} or 300 Å s^{-1}), due presumably to *g*-jitter disturbances, is a more serious concern for realizing the best quality protein crystals. Nevertheless, improvements in crystal perfection have been observed on a

number of microgravity shuttle missions and which are coming close to the theoretical limits of the rocking curve and spatial coherence of a protein crystal. The mimicking of microgravity, and thereby the matching on Earth of microgravity benchmark levels of quality is a key target; perhaps gel-based growth will provide these matching benchmarks. The full exploitation of such quality in X-ray crystallography is a challenge, and an opportunity, for computing and 'diffractometer' area-detector hardware. Such studies also require improved sample freezing techniques; the latter are essential to control X-ray damage to, but lead to less geometrical perfection of, the sample. A possible additional physical process for improved 'Bragg' diffraction data for microgravity-grown crystals is that disorder diffuse scattering (DDS) may be reduced. This has been seen in chemical crystallography for microgravity- versus Earth-grown crystals (Ahari *et al.* 1997), and may apply to protein crystals thus explaining why only a fraction of proteins and protein crystal types appear to benefit from microgravity (i.e. DDS is not commonly prevalent). Overall, improved crystal order via better crystal growth, and the understanding of the fluid physics which underpins it, will stimulate new developments in X-ray data collection and thereby data quality. Moreover, protein structure projects where only microcrystals can be grown, or perhaps projects with no crystals at all, might also benefit from these new developments in fluid physics and 'materials processing'.

Dr J. Stapelmann, R. Bosch, W. Fritzsch and W. Scheller of Dornier GmbH are thanked for their continuing help and support with this work and F. Bottcher for technical assistance. Dr H. U. Walter, Dr K. Fuhrmann, Dr H. Martinides and Dr O. Minster at ESA are acknowledged for their support and the opportunity to perform these experiments. The NSLS is acknowledged for providing beam time for the analysis of crystal perfection. The NSLS is funded by the US Department of Energy under contract number DE-AC02-76CH00016. Likewise the ESRF is thanked for provision of synchrotron radiation on BL19 and the undulator line BL4. The Wellcome Trust funded the Manchester R-AXIS to whom J.R.H. is grateful. J.D. was supported by the Royal Society for a one-year QE fellowship in Manchester on leave from Beijing. T.J.B. thanks the University of Manchester and the Samuel Hall fund for studentship support. The SRS is thanked for provision of synchrotron radiation on station 9.5 for ultra-long distance Laue mosaicity evaluation, as well as LURE and at the ESRF (Swiss–Norwegian beamline) for rocking curve measurement runs, results from which are described in the abstract.

References

Ahari, H., Bedard, R. L., Bowes, C. L., Coombs, N., Dag, Ö., Jiang, T., Ozin, G. A., Petrov, S., Sokolov, I., Verma, A., Vovk, G. & Young, D. 1997 Effect of microgravity on the crystallization of a self-assembling layered material. *Nature* **388**, 857–860.

Bi, R.-C. 1997 Protein crystal growth in space. In *Space science in China* (ed. W.-R. Hu), pp. 397–413. London: Gordon and Breach.

Boggon, T. J., Chayen, N. E., Zagalsky, P. F., Snell, E. H. & Helliwell, J. R. 1998 Stationary crystal growth of α-crustacyanin in microgravity onboard the unmanned EURECA carrier, monitored by video observation. *Acta Crystallogr.* D. (Submitted.)

Bosch, R., Lautenschlager, P., Potthast, L. & Stapelmann, J. 1992 Experimental equipment for protein crystallization in microgravity facilities. *J. Cryst. Growth* **122**, 310–316.

Chayen, N. E., Boggon, T. J., Cassetta, A., Deacon, A., Gleichmann, T., Habash, J., Harrop, S. J., Helliwell, J. R., Nieh, Y. P., Peterson, M. R., Raftery, J., Snell, E. H., Hädener, A., Niemann, A. C., Siddons, D. P., Stojanoff, V., Thompson, A. W., Ursby, T. & Wulff, M. 1996 Trends and challenges in experimental macromolecular crystallography. *Q. Rev. Biophys.* **29**, 227–278.

Chayen, N. E., Snell, E. H., Helliwell, J. R. & Zagalsky, P. F. 1997 CCD video observation of microgravity: apocrustacyanin C_1. *J. Cryst. Growth* **171**, 219–225.

Eilers, D. & Stark, H. R. 1993 EURECA microgravity environment: preliminary flight data. *NASA Conf. Proc.* **3272**, 869–891.

Helliwell, J. R. 1988 Protein crystal perfection and the nature of radiation damage. *J. Cryst. Growth*, **90**, 259–272.

Helliwell, J. R. 1992 *Macromolecular crystallography with synchrotron radiation*. Cambridge University Press.

Helliwell, J. R., Snell, E. H. & Weisgerber, S. 1996 An investigation of the perfection of lysozyme protein crystals grown in microgravity and on Earth. In *Proc. 1995 Berlin Microgravity Conf.* (ed. L. Ratke, H. U. Walter & B. Feuerbacher), pp. 155–170. Berlin: Springer.

Provost, K., & Robert, M. C. 1991 Application of gel growth to hanging drop technique. *J. Cryst. Growth* **110**, 258–264.

Riès-Kautt, M., Broutin, I., Ducruix, A., Shepard, W., Kahn, R., Chayen, N.E., Blow, D., Paal, K., Littke, W., Lorber, B., Théobald-Dietrich, A. & Giegé, R. 1997 Crystallogenesis studies in microgravity with the advanced protein crystallization facility on SpaceHab-01. *J. Cryst. Growth* **181**, 79–96.

Savino, R. & Monti, R. 1996 Buoyancy and surface-tension-driven convection in hanging-drop protein crystallizer. *J. Cryst. Growth* **165**, 308–318.

Schmidt, H. P., Koerver W. & Pätz, B. 1992 Practical aspects of crystal growth experiments on board EURECA-1. *J. Cryst. Growth* **122**, 317–322.

Snell, E. H. 1998 Quality evaluation of macromolecular crystals using X-ray mosaicity measurements. *Proc. Montreal Spacebound 97 Meeting, Canadian Space Agency.* (In the press.)

Snell, E. H., Weisgerber, S., Helliwell, J. R., Weckert, E., Hölzer, K. & Schroer, K. 1995 Improvements in lysozyme protein crystal perfection through microgravity growth. *Acta Crystallogr.* D **51**, 1099–1102.

Snell, E. H., Helliwell, J. R., Boggon, T. J., Lautenschlager, P. & Potthast, L. 1996 Lysozyme crystal growth kinetics monitored using a Mach–Zehnder interferometer. *Acta Crystallogr.* D **52**, 529–533.

Snell, E. H., Cassetta, A., Helliwell, J. R., Boggon, T. J., Chayen, N. E., Weckert, E., Hölzer, K., Schroer, K., Gordon, E. J. & Zagalsky, P. F. 1997*a* Partial improvement of crystal quality for microgravity grown apocrustacyanin C_1. *Acta Crystallogr.* D **53**, 231–239.

Snell, E. H., Boggon, T. J., Helliwell, J. R., Moskowitz M. E. & Nadarajah, A. 1997*b* CCD video observation of microgravity crystallization of lysozyme and correlation with accelerometer data. *Acta Crystallogr.* D **53**, 747–755.

Snyder, R. S., Fuhrmann, K. & Walter, H. U. 1991 Protein crystallization facilities for microgravity experiments. *J. Cryst. Growth* **110**, 333–338.

Stojanoff, V., Siddons, D. P., Snell, E. H. & Helliwell, J. R. 1996 X-ray topography: an old technique with a new application. *Synchrotron Radiation News* **9**, 25–26.

Stojanoff, V., Siddons, D. P., Monaco, L. A., Vekilov, P. G. & Rosenberger, F. 1997 X-ray topography of tetragonal lysozyme grown by the temperature controlled technique. *Acta. Crystallogr.* D **53**, 588–595.

Zagalsky, P. F., Wright, C. E. & Parsons, M. 1995 Crystallisation of α-crustacyanin, the lobster carapace astaxanthin-protein: results from EURECA. *Adv. Space Res.* **16**, 91–94.